### Title

Efficient high-speed cornering motions based on continuously-variable feedrates. I. Real-time interpolator algorithms




### Journal

The International Journal of Advanced Manufacturing Technology, 87(9-12)

### ISSN

0268-3768



### Authors

Farouki, Rida T
Nittler, Kevin M



### Publication Date

2016-12-01

### DOI

10.1007/s00170-016-8740-z

Peer reviewed

# Efficient high–speed cornering motions based on continuously–variable feedrates. I. Real–time interpolator algorithms

Rida T. Farouki and Kevin M. Nittler
Department of Mechanical and Aerospace Engineering,
University of California, Davis, CA 95616, USA.

**Abstract**

The problem of high–speed traversal of sharp toolpath corners, within a prescribed geometrical tolerance $\epsilon$, is addressed. Each sharp corner is replaced by a quintic Pythagorean–hodograph (PH) curve that meets the incoming/outgoing path segments with $G^2$ continuity, and deviates from the exact corner by no more than the prescribed tolerance $\epsilon$. The deviation and extremum curvature admit closed–form expressions in terms of the corner angle $\theta$ and side–length $L$, allowing precise control over these quantities. The PH curves also permit a smooth modulation of feedrate around the corner by analytic reduction of the interpolation integral. To demonstrate this, real–time interpolator algorithms are developed for three model feedrate functions. Specifying the feedrate as a quintic polynomial in the curve parameter accommodates precise acceleration continuity, but has no obvious geometrical interpretation. An inverse linear dependence on curvature offers a purely geometrical specification, but incurs slight initial and final tangential acceleration discontinuities. As an alternative, a hybrid form that incorporates the main advantages of these two approaches is proposed. In each case, the ratio $f = V_{\min}/V_0$ of the minimum and nominal feedrates is a free parameter, and the improved cornering time is analyzed. This paper develops the basic cornering algorithms — their implementation and performance analysis are described in detail in a companion paper.

**Keywords**: toolpath corner rounding; Pythagorean–hodograph curves;
CNC machines; continuously–variable feedrate; real–time interpolator algorithm.

e–mail: farouki@ucdavis.edu, kmnittler@ucdavis.edu

# 1 Introduction

The efficiency of common manufacturing processes, such as machining, laser cutting, and 3D printing, is often limited by the presence of sharp corners in part programs, which incur the need for large deceleration/acceleration rates to accurately negotiate corners. Since manufacturing costs directly correlate to part program execution times on high capital–investment equipment, it is desirable to minimize the time penalty incurred by cornering motions, while ensuring that the final part satisfies a prescribed tolerance $\epsilon$.

For a given machine physical configuration, the only possibilities for the reduction of cornering times are through modification of the control algorithm and/or part program geometry. A common approach is to replace each sharp corner by a smooth curve segment that deviates by no more than $\epsilon$ from the apex of the corner. This facilitates a reduction in cornering time through two effects: (a) the rounded corner has a shorter total path length than the sharp corner; and (b) since the rounded corner has finite extremum curvature, it becomes possible to maintain a non–zero feedrate over its entire extent rather than coming to a complete stop in the case of a sharp corner.

To fully exploit these effects, a corner rounding strategy should specify both the precise shape (i.e., curvature distribution) of the corner curve, and smooth variation of feedrate along it. Moreover, these specifications must be compatible with an accurate real–time interpolator algorithm, that is capable of generating precise reference points along the curved corner in accordance with the desired feedrate variation, at the controller sampling frequency. The *Pythagorean–hodograph* (PH) *curves* are eminently suited to this requirement [6, 7, 10, 18] and are the point of departure for the present study.

The focus of this paper is on rounding corners with significant angular deviations between contiguous linear segments. It is not intended to address real–time spline smoothing — or "compression" — of piecewise–linear G01 approximations to free–form toolpaths, that involve small angular deviations between short linear segments (such capability is already available in several commercial controllers). The goal is to mitigate the very high decelerations and accelerations incurred by discrete sharp corners through a modification of the corner geometry and an associated feedrate variation, allowing faster corner traversal while maintaining a prescribed geometrical tolerance. Also, for brevity, only planar toolpaths are addressed at present, but the extension to spatial toolpaths does not incur any exceptional difficulties.

Several authors have addressed the problem of rounding toolpath corners.

Šír and Jüttler [15] proposed the use of degree 9 $C^2$ PH Hermite interpolants [5] to round corners in planar tool paths, and extended these results to the spatial case in [16]. However, these studies address only the geometric aspect of the problem, and the formulation of real–time interpolators for variable feedrates along higher–order PH curves becomes rather complicated. Walton and Meek [19] noted that PH quintics can be constructed with specified end points and tangents, and zero end curvatures, that are well–suited to the $G^2$ blending of corners on piecewise–linear curves. The constructions described in Section 3 below are equivalent to those in [19], although use of the complex representation yields more compact formulations and easier analysis of key properties — extremum curvature, corner deviation, etc.

Ernesto and Farouki [2] used $G^1$ conic segments as corner rounding curves and formulated the problem of computing the feedrate variation along them, so as to minimize the traversal time under prescribed axis acceleration bounds, as a calculus of variations problem with pointwise constraints. Exploiting the convex hull and subdivision properties of the Bernstein form, a sequence of approximations that converge to the exact solution are obtained by solving a sequence of linear programming problems. Shi et al. [13] considered the use of $G^2$ PH quintic corner curves for high–speed machining, and extended this to the context of 5–axis machining in [14]. Sencer et al. [12] used "ordinary" quintic Bézier curves as $G^2$ rounded corners, whose maximum curvature is minimized with respect to residual free parameters. In executing the corners, a reduction $\Delta V$ of the nominal feedrate $V$ along linear segments is used, with smooth "S-shaped" transitions between the nominal/reduced values.

A key advantage of the PH curves, in the context of the corner–rounding problem, is the ability to formulate real–time CNC interpolator algorithms that correspond to *continuously–variable* feedrates. A feedrate dependent on the path curvature can, for example, ensure that centripetal acceleration is kept within acceptable limits. An investigation of the use of this capability, in the context of high–speed motion control, is the main focus of this study. The present paper develops the mathematical formulations and algorithms required for the construction and analysis of the $G^2$ PH quintic corner curves, and real–time interpolator algorithms for representative feedrate variations. A companion paper [11] presents detailed results from an implementation on a 3–axis CNC milling machine with an open–architecture contoller.

The plan for the remainder of this paper is as follows. Section 2 reviews some basic properties of planar PH curves, and their advantageous features in the context of the corner rounding problem. The construction of a single

PH quintic corner curve that exhibits second–order geometric continuity with the incoming and outgoing linear segments, and accommodates a general side length $L$ and corner angle $\theta$, is then treated in Section 3. The key properties of the PH quintic corner curves are also derived in Section 3 — the parametric speed and arc length polynomials, curvature variation and extremum, and maximum deviation from the original sharp corner.

Real–time interpolator algorithms for three feedrate variations associated with these $G^2$ PH quintic corner curves are then formulated in Sections 4–6. The first case employs a feedrate defined as a quintic polynomial in the curve parameter, incorporating a single coefficient $f$ that specifies the mid–point feedrate $V_{\min}$ as a fraction of the nominal value $V_0$. The second case employs a feedrate expressed as a simple function of curvature, that admits a closed–form reduction of the interpolation integral, with $f$ freely chosen. However, it incurs slight tangential acceleration discontinuities, since the feedrate has non–zero derivative at the end–points. Finally, the third case is a hybrid of the first two, in which a quadratic factor in the curve parameter is invoked to modulate the curvature so as to achieve acceleration continuity.

For each of the feedrate variations, the dependence of the corner traversal time on the quantities $f$, $L$, $\theta$ is analyzed, relative to a nominal value for the sharp corner. Finally, Section 7 analyzes the accelerations of the individual machine axes incurred by the cornering strategies (with an emphasis on the first feedrate function), while Section 8 recapitulates the main points of this study and directs the reader to the companion paper [11].

# 2 Planar Pythagorean–hodograph curves

A planar polynomial Pythagorean–hodograph (PH) curve $\mathbf{r}(\xi) = (x(\xi), y(\xi))$ is distinguished by the special property that its derivative $\mathbf{r}'(\xi) = (x'(\xi), y'(\xi))$ has components satisfying [9] the Pythagorean condition

$$x'^2(\xi) + y'^2(\xi) \;=\; \sigma^2(\xi) \tag{1}$$

for some polynomial $\sigma(\xi)$, which defines the *parametric speed* of $\mathbf{r}(\xi)$ — i.e., the derivative $\mathrm{d}s/\mathrm{d}\xi$ of arc length $s$ with respect to the curve parameter $\xi$. The fact that $\sigma(\xi)$ is a polynomial (and not the square root of a polynomial) endows PH curves with several attractive computational properties.

For a primitive curve with $\gcd(x'(\xi), y'(\xi)) = \text{constant}$, a sufficient and necessary condition for satisfaction of (1) is that the derivative components

should be expressible in the form

$$x'(\xi) \;=\; u^2(\xi) - v^2(\xi)\,, \quad y'(\xi) \;=\; 2\,u(\xi)v(\xi)\,,$$

where $u(\xi)$, $v(\xi)$ are polynomials with $\gcd(u(\xi), v(\xi)) = \text{constant}$. This form is embodied in the *complex representation* [3], in which a PH curve of degree $n = 2m + 1$ is generated from a degree–$m$ complex polynomial

$$\mathbf{w}(\xi) \;=\; u(\xi) + \mathrm{i}\,v(\xi) \;=\; \sum_{k=0}^{m} \mathbf{w}_k \binom{m}{k} (1-\xi)^{m-k}\xi^k \tag{2}$$

with Bernstein coefficients $\mathbf{w}_k = u_k + \mathrm{i}\,v_k$ by integrating the expression

$$\mathbf{r}'(\xi) \;=\; \mathbf{w}^2(\xi)\,. \tag{3}$$

The parametric speed of $\mathbf{r}(\xi)$ is $\sigma(\xi) = |\mathbf{w}(\xi)|^2$, and its unit tangent, unit normal, and curvature may be expressed [3] in terms of $\mathbf{w}(\xi)$ as

$$\mathbf{t}(\xi) \;=\; \frac{\mathbf{w}^2(\xi)}{\sigma(\xi)}\,, \quad \mathbf{n}(\xi) \;=\; -\,\mathrm{i}\,\frac{\mathbf{w}^2(\xi)}{\sigma(\xi)}\,, \quad \kappa(\xi) \;=\; 2\,\frac{\mathrm{Im}(\overline{\mathbf{w}}(\xi)\mathbf{w}'(\xi))}{\sigma^2(\xi)}\,. \tag{4}$$

Since $\sigma(\xi) = u^2(\xi) + v^2(\xi)$ is a polynomial, the cumulative arc length function

$$s(\xi) \;=\; \int_0^{\xi} \sigma(\tau)\;\mathrm{d}\tau$$

is likewise a polynomial in $\xi$. These facts facilitate development of essentially exact *real–time interpolator* algorithms for PH curves, for feedrates (speeds) dependent of arc length, time, curvature, etc. [6, 7, 10, 18].

For a specified feedrate $V$ along $\mathbf{r}(\xi)$, the acceleration $\mathbf{a}$ is the derivative of the velocity $\mathbf{v} = V\mathbf{t}$ with respect to time $t$. Using

$$\frac{\mathrm{d}V}{\mathrm{d}t} \;=\; \frac{\mathrm{d}s}{\mathrm{d}t}\frac{\mathrm{d}\xi}{\mathrm{d}s}\frac{\mathrm{d}V}{\mathrm{d}\xi} \;=\; \frac{VV'}{\sigma} \qquad \text{and} \qquad \frac{\mathrm{d}\mathbf{t}}{\mathrm{d}t} \;=\; \frac{\mathrm{d}s}{\mathrm{d}t}\frac{\mathrm{d}\mathbf{t}}{\mathrm{d}s} \;=\; -V\kappa\,\mathbf{n}\,,$$

we obtain

$$\mathbf{a}(\xi) \;=\; \frac{V(\xi)V'(\xi)}{\sigma(\xi)}\,\mathbf{t}(\xi) \;-\; \kappa(\xi)V^2(\xi)\,\mathbf{n}(\xi)\,. \tag{5}$$

The first term in (5) is the *tangential* or *feed acceleration*, equal in magnitude to the time derivative of the feedrate, while the second term is the *normal* or *centripetal acceleration*, whose magnitude is equal to the product of the curvature and the square of the feedrate.

# 3 Canonical $G^2$ PH quintic corner

Consider the rounding of two linear segments that meet at a corner point $\mathbf{p}_c$. The sharp corner is to be replaced by a smooth curve $\mathbf{r}(\xi)$, $\xi \in [\,0,1\,]$ that begins at a point $\mathbf{p}_i$ on the incoming line segment, and ends at a point $\mathbf{p}_o$ on the outgoing line segment, i.e.,

$$\mathbf{r}(0) \;=\; \mathbf{p}_i \qquad \text{and} \qquad \mathbf{r}(1) \;=\; \mathbf{p}_o\,,$$

where we require $|\mathbf{p}_c - \mathbf{p}_i| = |\mathbf{p}_o - \mathbf{p}_c|$ for symmetry. Furthermore, to ensure a $G^2$ connection with the line segments, the tangent $\mathbf{t}(\xi)$ and curvature $\kappa(\xi)$ of $\mathbf{r}(\xi)$ must satisfy

$$\mathbf{t}(0) \;=\; \frac{\mathbf{p}_c - \mathbf{p}_i}{|\mathbf{p}_c - \mathbf{p}_i|}\,, \quad \mathbf{t}(1) \;=\; \frac{\mathbf{p}_o - \mathbf{p}_c}{|\mathbf{p}_o - \mathbf{p}_c|}\,, \quad \kappa(0) \;=\; \kappa(1) \;=\; 0\,.$$

For simplicity, this problem is considered for "canonical" data, of the form

$$\mathbf{p}_i \;=\; (0,0)\,, \quad \mathbf{p}_c \;=\; (L,0)\,, \quad \mathbf{p}_o \;=\; ((1+\cos\theta)L, \sin\theta\, L)\,,$$

for $-\pi < \theta < +\pi$ with $\theta \neq 0$ (see Figure 1). Note that the "turning angle" $\theta$ is measured positive anti–clockwise. The solution for arbitrary data $\mathbf{p}_i, \mathbf{p}_c, \mathbf{p}_o$ with $|\mathbf{p}_c - \mathbf{p}_i| = |\mathbf{p}_o - \mathbf{p}_c| \neq 0$ is obtained from the canonical solution through a rotation and translation. The translation amounts to simply choosing the initial Bézier control point $\mathbf{p}_0$ in expressions (7) below, while the rotation is achieved by multiplying the complex coefficients $\mathbf{w}_0, \mathbf{w}_1, \mathbf{w}_2$ of the polynomial (6) below by $\exp(\mathrm{i}\frac{1}{2}\phi)$, where $\phi$ is the angle such that

$$\cos\phi \;=\; \frac{x_c - x_i}{|\mathbf{p}_c - \mathbf{p}_i|}\,, \quad \sin\phi \;=\; \frac{y_c - y_i}{|\mathbf{p}_c - \mathbf{p}_i|}\,,$$

and we write $\mathbf{p}_i = (x_i, y_i)$ and $\mathbf{p}_c = (x_c, y_c)$. The translation and rotation do not affect the expressions derived below for the parametric speed (16), corner deviation (17), arc length (18), curvature (19), and also the variable–feedrate real–time interpolator algorithms developed in Sections 4–6.

The $G^2$ corner–rounding problem can be solved using a single PH quintic segment. Consider the PH quintic $\mathbf{r}(\xi)$ defined on $\xi \in [\,0,1\,]$ by substituting a quadratic complex polynomial

$$\mathbf{w}(\xi) \;=\; \mathbf{w}_0(1-\xi)^2 + \mathbf{w}_1 2(1-\xi)\xi + \mathbf{w}_2\xi^2 \tag{6}$$

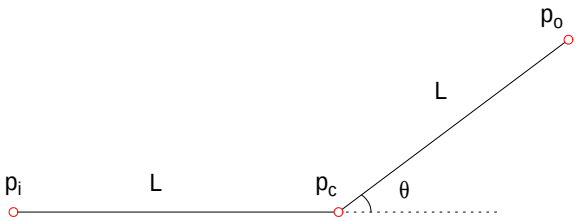


Figure 1: Canonical data for the $G^2$ PH quintic corner curve.

into (3) and integrating. The Bézier control points of $\mathbf{r}(\xi)$ are determined [4] from the coefficients $\mathbf{w}_0, \mathbf{w}_1, \mathbf{w}_2$ as

$$\begin{aligned}
\mathbf{p}_1 &= \mathbf{p}_0 + \frac{1}{5}\,\mathbf{w}_0^2\,, \\
\mathbf{p}_2 &= \mathbf{p}_1 + \frac{1}{5}\,\mathbf{w}_0\mathbf{w}_1\,, \\
\mathbf{p}_3 &= \mathbf{p}_2 + \frac{1}{5}\,\frac{2\mathbf{w}_1^2 + \mathbf{w}_0\mathbf{w}_2}{3}\,, \\
\mathbf{p}_4 &= \mathbf{p}_3 + \frac{1}{5}\,\mathbf{w}_1\mathbf{w}_2\,, \\
\mathbf{p}_5 &= \mathbf{p}_4 + \frac{1}{5}\,\mathbf{w}_2^2\,,
\end{aligned} \tag{7}$$

$\mathbf{p}_0$ being a free integration constant. The end tangents and end curvatures of $\mathbf{r}(\xi)$ must satisfy

$$\mathbf{t}(0) \;=\; \frac{\mathbf{w}_0^2}{|\mathbf{w}_0|^2} \;=\; 1\,, \qquad \mathbf{t}(1) \;=\; \frac{\mathbf{w}_2^2}{|\mathbf{w}_2|^2} \;=\; \exp(\mathrm{i}\,\theta)\,, \tag{8}$$

$$\kappa(0) \;=\; 4\,\frac{\mathrm{Im}(\overline{\mathbf{w}}_0\mathbf{w}_1)}{|\mathbf{w}_0|^4} \;=\; 0\,, \qquad \kappa(1) \;=\; 4\,\frac{\mathrm{Im}(\overline{\mathbf{w}}_1\mathbf{w}_2)}{|\mathbf{w}_2|^4} \;=\; 0\,. \tag{9}$$

The conditions (8) together with $|\mathbf{p}_c - \mathbf{p}_i| = |\mathbf{p}_o - \mathbf{p}_c| = L$ imply that $\mathbf{w}_0, \mathbf{w}_2$ must be of the form

$$\mathbf{w}_0 \;=\; \lambda\,\sqrt{L}\,, \quad \mathbf{w}_2 \;=\; \mu\,\sqrt{L}\,\exp(\mathrm{i}\tfrac{1}{2}\theta) \tag{10}$$

for non–zero real values $\lambda, \mu$ (we may assume that $\lambda > 0$, since the curve $\mathbf{r}(\xi)$ remains unchanged upon replacing $\mathbf{w}_0, \mathbf{w}_1, \mathbf{w}_2$ by $-\mathbf{w}_0, -\mathbf{w}_1, -\mathbf{w}_2$). Setting $\mathbf{w}_1 = u_1 + \mathrm{i}\,v_1$ and substituting for $\mathbf{w}_0, \mathbf{w}_2$ into the constraints (9) then gives

$$\lambda v_1 \;=\; \mu\,(u_1 \sin\tfrac{1}{2}\theta - v_1 \cos\tfrac{1}{2}\theta) \;=\; 0\,.$$

Since $\lambda, \mu$ must be non–zero, and by assumption $\theta \neq 2k\pi$ for integer $k$, these equations imply that $u_1 = v_1 = 0$ — i.e.,

$$\mathbf{w}_1 \;=\; 0\,. \tag{11}$$

From (7) we then have $\mathbf{p}_2 = \mathbf{p}_1$ and $\mathbf{p}_4 = \mathbf{p}_3$, so the $G^2$ corner has just four distinct control points instead of six [3]. The fact that $\mathbf{w}_1 = 0$ for any PH quintic satisfying $\kappa(0) = \kappa(1) = 0$ has been noted in Theorem 5.1 of [19].

With $\mathbf{p}_0 = \mathbf{p}_i$ and $\mathbf{p}_5 = \mathbf{p}_o$, interpolation of the corner end points yields the condition

$$\begin{aligned}\int_0^1 \mathbf{r}'(\xi)\,\mathrm{d}\xi \;&=\; \frac{1}{5}\left[\mathbf{w}_0^2 + \mathbf{w}_0\mathbf{w}_1 + \frac{2\mathbf{w}_1^2 + \mathbf{w}_0\mathbf{w}_2}{3} + \mathbf{w}_1\mathbf{w}_2 + \mathbf{w}_2^2\right] \\ &=\; L(1 + \cos\theta + \mathrm{i}\sin\theta)\,.\end{aligned}$$

On substituting from (10) and (11) for $\mathbf{w}_0, \mathbf{w}_1, \mathbf{w}_2$ the real and imaginary parts of this equation become

$$\begin{aligned}3\lambda^2 + \cos\tfrac{1}{2}\theta\,\lambda\mu + 3\cos\theta\,\mu^2 \;&=\; 15\,(1 + \cos\theta)\,, \\ \sin\tfrac{1}{2}\theta\,\lambda\mu + 3\sin\theta\,\mu^2 \;&=\; 15\,\sin\theta\,.\end{aligned}$$

Writing $\cos\theta = 2\cos^2\tfrac{1}{2}\theta - 1$, $\sin\theta = 2\sin\tfrac{1}{2}\theta\cos\tfrac{1}{2}\theta$ and noting that $\sin\tfrac{1}{2}\theta \neq 0$, we obtain

$$\begin{aligned}3\lambda^2 + \cos\tfrac{1}{2}\theta\,\lambda\mu + 3(2\cos^2\tfrac{1}{2}\theta - 1)\,\mu^2 \;&=\; 30\,\cos^2\tfrac{1}{2}\theta\,, \\ \lambda\mu + 6\cos\tfrac{1}{2}\theta\,\mu^2 \;&=\; 30\,\cos\tfrac{1}{2}\theta\,. \end{aligned}\tag{12}$$

The second equation gives

$$\lambda \;=\; \frac{6\cos\tfrac{1}{2}\theta\,(5 - \mu^2)}{\mu}\,, \tag{13}$$

and substituting this into the first equation yields the biquadratic

$$(36\cos^2\tfrac{1}{2}\theta - 1)\,\mu^4 - 360\cos^2\tfrac{1}{2}\theta\,\mu^2 + 900\cos^2\tfrac{1}{2}\theta \;=\; 0\,,$$

in $\mu$, from which we obtain

$$\mu^2 \;=\; \frac{30\cos\tfrac{1}{2}\theta}{6\cos\tfrac{1}{2}\theta \pm 1}\,. \tag{14}$$

Noting that $\cos\frac{1}{2}\theta > 0$ for $-\pi < \theta < +\pi$ (with $\theta \neq 0$), a real solution $\mu$ is possible only when $\cos\frac{1}{2}\theta > \frac{1}{6}$ if the $-$ sign is chosen in (14). Although the resulting curves match the prescribed end points, tangents, and curvatures when this condition is satisfied, they exhibit undesired loops. We therefore discard these solutions and use only the $+$ sign in (14), which yields a real solution $\mu$ for any $\theta$. Substituting it into (13), we obtain

$$\lambda \;=\; \mu \;=\; \sqrt{\frac{30\cos\frac{1}{2}\theta}{6\cos\frac{1}{2}\theta + 1}}\,. \tag{15}$$

Hence, the solutions to (12) define a symmetric curve, with $|\mathbf{r}'(1)| = |\mathbf{r}'(0)|$. From (7) and (10)–(11), the Bézier control points of the canonical PH quintic rounded corner can be expressed as

$$\mathbf{p}_0 \;=\; (0,0)\,, \quad \mathbf{p}_1 \;=\; \mathbf{p}_2 \;=\; \left(\frac{6L\cos\frac{1}{2}\theta}{6\cos\frac{1}{2}\theta + 1}, 0\right)\,,$$

$$\mathbf{p}_3 \;=\; \mathbf{p}_4 \;=\; \left(L + \frac{L\cos\theta}{6\cos\frac{1}{2}\theta + 1}, \frac{L\sin\theta}{6\cos\frac{1}{2}\theta + 1}\right)\,, \quad \mathbf{p}_5 \;=\; (L + L\cos\theta, L\sin\theta)\,.$$

Examples of the PH quintic corner curves, together with their Bézier control polygons and curvature profiles, are illustrated in Figure 2.

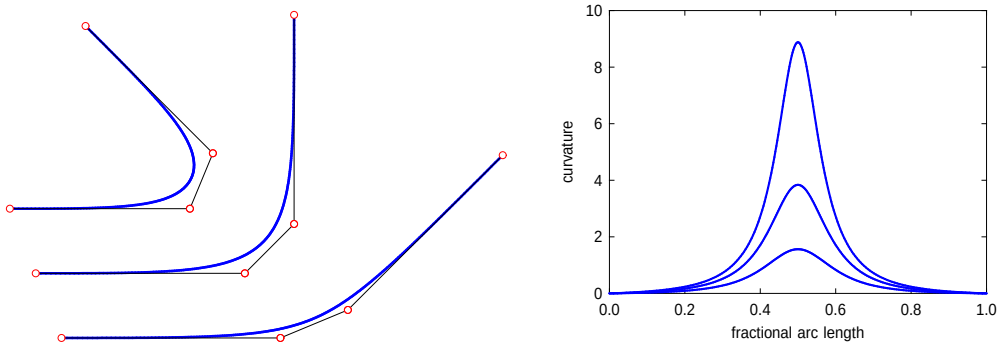


Figure 2: Left: examples of the canonical $G^2$ PH quintic corner curve, with their Bézier control polygons, for the three turning angles $\theta = \frac{1}{4}\pi, \frac{1}{2}\pi, \frac{3}{4}\pi$. Right: the curvature distributions for these three PH quintic corner curves.

The parametric speed is defined by the quartic polynomial

$$\sigma(\xi) \;=\; \sum_{k=0}^{4} \sigma_k \binom{4}{k} (1-\xi)^{4-k}\xi^k$$

with Bernstein coefficients

$$\begin{aligned}\sigma_0 &= |\mathbf{w}_0|^2, \quad \sigma_1 = \mathrm{Re}(\overline{\mathbf{w}}_0\mathbf{w}_1)\,,\\ \sigma_2 &= [\,2|\mathbf{w}_1|^2 + \mathrm{Re}(\overline{\mathbf{w}}_0\mathbf{w}_2)\,]/3\,,\\ \sigma_3 &= \mathrm{Re}(\overline{\mathbf{w}}_1\mathbf{w}_2)\,, \quad \sigma_4 = |\mathbf{w}_2|^2\,.\end{aligned}$$

Substituting for $\mathbf{w}_0, \mathbf{w}_1, \mathbf{w}_2$ gives $\sigma_1 = \sigma_3 = 0$ and

$$\sigma_0 = \sigma_4 = \lambda^2 L = \frac{30L\cos\frac{1}{2}\theta}{6\cos\frac{1}{2}\theta + 1}\,, \qquad \sigma_2 = \frac{\lambda^2 L\cos\frac{1}{2}\theta}{3} = \frac{10L\cos^2\frac{1}{2}\theta}{6\cos\frac{1}{2}\theta + 1}\,.$$

Hence, the parametric speed can be expressed as

$$\sigma(\xi) = \lambda^2 L\,[\,(1-\xi)^4 + 2\cos\tfrac{1}{2}\theta\,(1-\xi)^2\xi^2 + \xi^4\,]\,. \tag{16}$$

It decreases from $\sigma(0) = \sigma(1) = \lambda^2 L$ at the end points to the minimum value $\sigma(\frac{1}{2}) = \frac{1}{8}\lambda^2 L(1+\cos\frac{1}{2}\theta)$ at the mid–point of the corner curve. The mid–point has coordinates

$$\mathbf{r}(\tfrac{1}{2}) = L\left(1 - \frac{3\cos\frac{1}{2}\theta + 8}{16(6\cos\frac{1}{2}\theta + 1)}(1-\cos\theta), \frac{3\cos\frac{1}{2}\theta + 8}{16(6\cos\frac{1}{2}\theta + 1)}\sin\theta\right)\,,$$

and hence its deviation $\delta$ from the corner point $\mathbf{p}_c = (1,0)$ is

$$\delta(\theta) = |\,\mathbf{r}(\tfrac{1}{2}) - (1,0)\,| = \frac{(3\cos\frac{1}{2}\theta + 8)\,|\sin\frac{1}{2}\theta\,|\,L}{8(6\cos\frac{1}{2}\theta + 1)}\,, \tag{17}$$

as illustrated in Figure 3. It has limiting values $\delta \to 0$ and $\delta \to L$ as $\theta \to 0$ and $\theta \to \pi$, respectively, the intermediate value for a right–angle turn being

$$\delta(\tfrac{1}{2}\pi) = \frac{45+\sqrt{2}}{272}\,L \approx 0.170640\,L\,.$$

The cumulative arc length function for the $G^2$ PH quintic corner is

$$s(\xi) = \int_0^\xi \sigma(\tau)\,\mathrm{d}\tau = \sum_{k=0}^{5} s_k \binom{5}{k}(1-\xi)^{5-k}\xi^k\,,$$

where

$$s_0 = 0 \qquad \text{and} \qquad s_k = s_{k-1} + \frac{\sigma_{k-1}}{5}\,, \quad k = 1,\ldots,5\,.$$

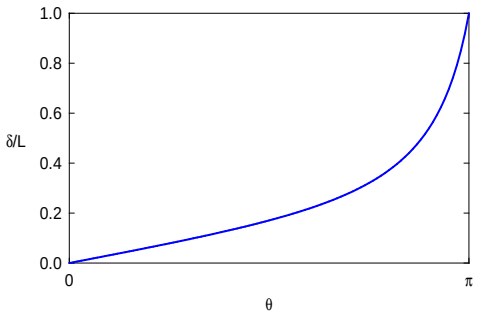


Figure 3: The deviation (17) of the canonical $G^2$ PH quintic rounded corner curve from the exact corner as a function of the turning angle $\theta$.

In particular, the total arc length is

$$S \;=\; \frac{\sigma_0 + \sigma_1 + \sigma_2 + \sigma_3 + \sigma_4}{5} \;=\; \frac{2L(6 + \cos\frac{1}{2}\theta)\cos\frac{1}{2}\theta}{6\cos\frac{1}{2}\theta + 1}\,. \tag{18}$$

Finally, the curvature of the PH quintic corner curve can be expressed as

$$\kappa(\xi) \;=\; 4\,\mathrm{Im}(\overline{\mathbf{w}}_0\mathbf{w}_2)\,\frac{(1-\xi)\xi}{\sigma^2(\xi)} \;=\; 4\,\lambda^2 L \sin\tfrac{1}{2}\theta\,\frac{(1-\xi)\xi}{\sigma^2(\xi)}\,. \tag{19}$$

Note that $\kappa(\xi)$ is either positive or negative for $\xi \in (0,1)$ according to whether $\theta$ is positive or negative, i.e., whether the specified points $\mathbf{p}_i$, $\mathbf{p}_c$, $\mathbf{p}_o$ define a "left–turn" or "right–turn" corner. It vanishes at the curve end points, and has the mid–point extremum value

$$\kappa_{\max} \;=\; \kappa(\tfrac{1}{2}) \;=\; \frac{32(6\cos\frac{1}{2}\theta + 1)\tan\frac{1}{2}\theta}{15L(\cos\frac{1}{2}\theta + 1)^2}\,. \tag{20}$$

Figure 4 illustrates the variation of the total arc length $S$ and the extremum curvature $\kappa_{\max}$ with the corner angle $\theta$.

# 4 Parameter-dependent feedrate

Consider a cornering feedrate specified as a quintic polynomial

$$V(\xi) \;=\; \sum_{k=0}^{5} v_k \binom{5}{k} (1-\xi)^{5-k}\xi^k \tag{21}$$

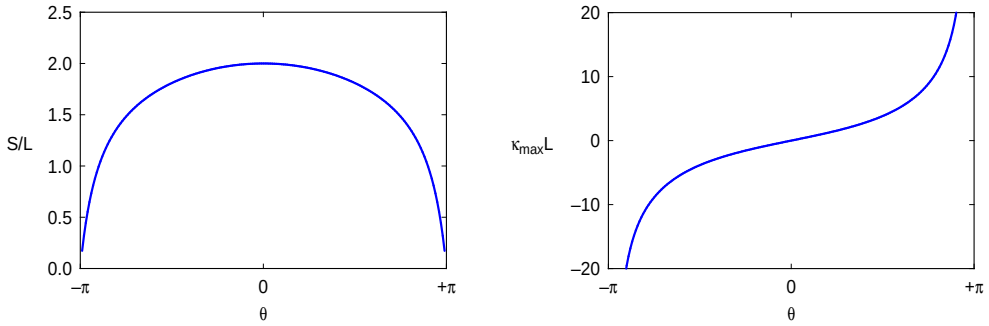


Figure 4: Variation of total arc length $S$ (left) and extremum curvature $\kappa_{\max}$ (right) with the turning angle $\theta$ of the $G^2$ PH quintic rounded corner curve.

in the curve parameter. To ensure continuity of velocity and acceleration, the conditions $V(0) = V(1) = V_0$ and $V'(0) = V'(1) = 0$ are imposed. If we also stipulate that the minimum feedrate $V(\frac{1}{2}) = V_{\min}$ at the curve mid–point is a specified fraction $f$ of $V_0$, the coefficients of (21) are determined as

$$v_0 = v_1 = v_4 = v_5 = V_0\,, \qquad v_2 = v_3 = \frac{8f-3}{5}\,V_0\,. \tag{22}$$

Using these values and the partition–of–unity property of the Bernstein form, the feedrate (21) can also be expressed as

$$V(\xi) \;=\; V_0\,[\,1 - 16(1-f)(1-\xi)^2\xi^2\,]\,, \tag{23}$$

so $V(\xi)$ is actually quartic. Figure 5 shows the feedrate variation in the case $\theta = \frac{1}{2}\pi$ for various values of $f$ (the cases $\theta = \frac{1}{4}\pi$ and $\frac{3}{4}\pi$ are very similar).

Since the feedrate and parametric speed are the derivatives of arc length $s$ with respect to time $t$ and the curve parameter $\xi$, the time variation of $\xi$ is determined from the chain–rule relation

$$\frac{\mathrm{d}\xi}{\mathrm{d}t} \;=\; \frac{\mathrm{d}\xi}{\mathrm{d}s}\frac{\mathrm{d}s}{\mathrm{d}t} \;=\; \frac{V(\xi)}{\sigma(\xi)}\,. \tag{24}$$

Subsituting from (23), the parameter value $\xi_k$ of the reference point at time $t = k\Delta t$ is determined from the condition

$$\int_0^{\xi_k} \frac{\sigma(\xi)}{1 - 16(1-f)(1-\xi)^2\xi^2}\;\mathrm{d}\xi \;=\; V_0 k\Delta t\,. \tag{25}$$

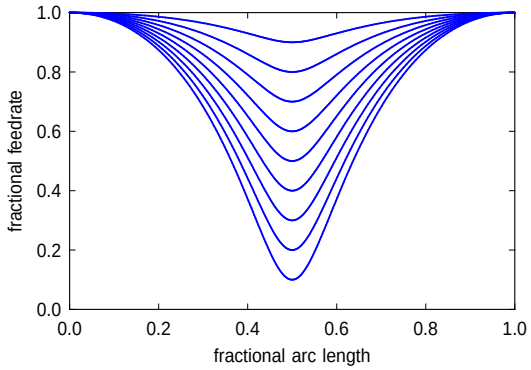


Figure 5: Fractional feedrate $V/V_0$ versus arc length $s/S$ for the acceleration–continuous feedrate defined by (21) and (22) with $f = V_{\min}/V_0 = 0.1, \ldots, 0.9$.

Now using (16) and the factorization

$$1 - 16(1-f)(1-\xi)^2\xi^2 \;=\; [\,1 + 4c(1-\xi)\xi)\,]\,[\,1 - 4c(1-\xi)\xi\,]\,,$$

the integrand in (25) has the partial fraction decomposition

$$\frac{\lambda^2 L}{16c^2}\left[\,\frac{a}{1+4c(1-\xi)\xi} + \frac{b}{1-4c(1-\xi)\xi} - 2(1+\cos\tfrac{1}{2}\theta)\,\right], \qquad (26)$$

where we define

$$a = 8c^2 + 8c + 1 + \cos\tfrac{1}{2}\theta\,, \quad b = 8c^2 - 8c + 1 + \cos\tfrac{1}{2}\theta\,, \quad c = \sqrt{1-f}\,.$$

Writing

$$p \;=\; \frac{\sqrt{c+c^2}}{c} \;=\; \left[\frac{1}{\sqrt{1-f}} + 1\right]^{1/2}, \quad q \;=\; \frac{\sqrt{c-c^2}}{c} \;=\; \left[\frac{1}{\sqrt{1-f}} - 1\right]^{1/2},$$

the expression (26) has the indefinite integral

$$\frac{\lambda^2 L}{16c^2}\left[\,\frac{a}{4cp}\ln\frac{1-2\xi-p}{1-2\xi+p} + \frac{b}{2cq}\tan^{-1}\frac{2\xi-1}{q} - 2(1+\cos\tfrac{1}{2}\theta)\,\xi\,\right].$$

Hence, evaluating the integral between limits 0 and $\xi_k$, the reference–point parameter value $\xi_k$ at time $t = k\Delta t$ is the real root of the equation

$$F(\xi) \;=\; \frac{\lambda^2 L}{16c^2}\left[\,\frac{a}{4cp}\ln\frac{1+2c(p+1)\xi}{1-2c(p-1)\xi} + \frac{b}{2cq}\left(\tan^{-1}\frac{2\xi-1}{q} + \tan^{-1}\frac{1}{q}\right)\right.$$
$$\left. -\; 2(1+\cos\tfrac{1}{2}\theta)\,\xi\,\right] - V_0 k\Delta t \;=\; 0\,.$$

Since this function is monotone–increasing on $\xi \in [\,0,1\,]$ it has a unique root on that interval, which can be computed to machine precision through a few Newton–Raphson iterations

$$\xi_k^{(r)} \;=\; \xi_k^{(r-1)} \;-\; \frac{F(\xi_k^{(r-1)})}{F'(\xi_k^{(r-1)})}\,, \qquad r = 1, 2, \ldots \tag{27}$$

from the starting approximation

$$\xi_k^{(0)} \;=\; \xi_{k-1} + \frac{V(\xi_{k-1})\Delta t}{\sigma(\xi_{k-1})}\,, \tag{28}$$

where $\xi_{k-1}$ is the converged value from the previous timestep. Convergence to machine precision is typically observed in just 2 or 3 iterations. Note that the derivative of $F(\xi)$ required in (27) is

$$F'(\xi) \;=\; \frac{\sigma(\xi)}{1 - 16(1-f)(1-\xi)^2\xi^2}\,.$$

Figure 6 illustrates the distribution of reference points along some PH quintic corners, using the parameter–dependent feedrate defined by (21)–(22).

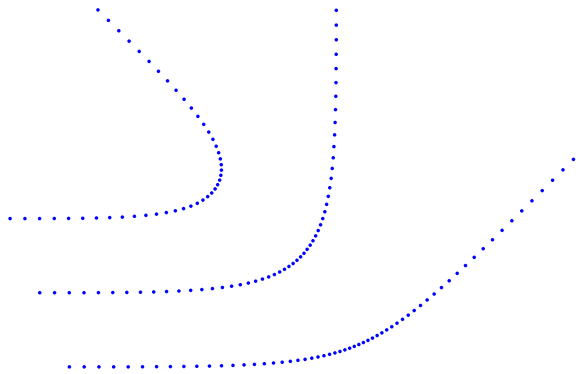

Figure 6: The distribution of reference points along $G^2$ PH quintic corners with turning angles $\theta = \frac{1}{4}\pi, \frac{1}{2}\pi, \frac{3}{4}\pi$ using the acceleration–continuous feedrate (21) with the values $L = 1$ mm, $V_0 = 50$ mm/sec, $\Delta t = 0.001$ sec, and $f = \frac{1}{3}$.

For the feedrate (23), the PH quintic corner traversal time $T$ is obtained by replacing $\xi_k$ with 1 and $k\Delta t$ with $T$ in (25) as

$$\frac{T}{T_0} \;=\; \frac{\lambda^2}{64c^2}\left[\,\frac{a}{4cp}\ln\frac{1+2c(p+1)}{1-2c(p-1)} \;+\; \frac{b}{cq}\tan^{-1}\frac{1}{q} \;-\; 2(1+\cos\tfrac{1}{2}\theta)\,\right] \tag{29}$$

where $c, p, q$ are defined in terms of $f$ as before, and $T_0 = 4L/V_0$ is the sharp corner traversal time with uniform deceleration/acceleration. The ratio (29) is plotted as a function of $f$ in Figure 7 — for typical angles, it is seen that values $f \geq \frac{1}{2}$ give reductions of $\sim 50\%$ in the cornering time.

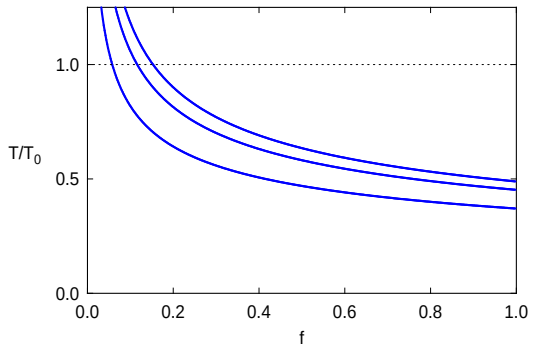


Figure 7: The corner traversal time ratio (29) as a function of the feedrate suppression factor $f$ for three representative corner angles: $\theta = \frac{1}{4}\pi,\ \frac{1}{2}\pi,\ \frac{3}{4}\pi$ (the uppermost graph is for the smallest $\theta$, the lowermost for the largest $\theta$).

# 5 Curvature–dependent feedrate

For a specified linear feedrate $V_0$, consider the curvature–dependent cornering feedrate function

$$V(\xi) \;=\; \frac{V_0}{\rho\,\kappa(\xi) + 1}\,, \tag{30}$$

where $\rho$ is a signed length scale, used to determine the severity of the corner feedrate suppression. To obtain a mid–point minimum feedrate $V_{\min} = V(\frac{1}{2})$ as a desired fraction $f$ of the nominal feedrate $V_0$, we use the value

$$\rho \;=\; \frac{1-f}{f}\,r_{\min}\,, \tag{31}$$

where $r_{\min} = 1/\kappa_{\max}$ is the extremum corner radius of curvature. Note that $r_{\min}$ and $\rho$ are of the same sign as $\kappa(\xi)$ defined by (20), so the product $\rho\,\kappa(\xi)$ is positive for $0 < \xi < 1$. Since $\kappa(0) = \kappa(1) = 0$, the feedrate (30) decreases from $V_0$ at $\xi = 0$, to $V_{\min} = f\,V_0$ at $\xi = \frac{1}{2}$, and increases again to $V_0$ at $\xi = 1$.

Figure 8 illustrates the variation of the curvature–dependent feedrate (30) with fractional arc length along the $G^2$ PH quintic corner, for several values of the feedrate suppression factor $f = V_{\min}/V_0$ (the corner angle is $\theta = \frac{1}{2}\pi$ is shown here: the cases $\theta = \frac{1}{4}\pi$ and $\frac{3}{4}\pi$ are quite similar).

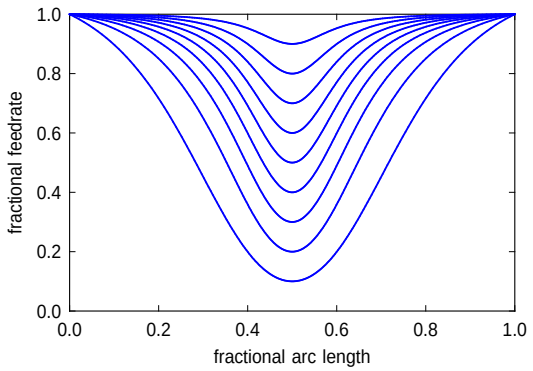


Figure 8: Fractional feedrate $V/V_0$ versus arc length $s/S$ for the curvature–dependent feedrate function (30) with the values $f = V_{\min}/V_0 = 0.1, \ldots, 0.9$.

Substituting from (19) and (30) into (24) and simplifying gives

$$\frac{\mathrm{d}\xi}{\mathrm{d}t} \;=\; \frac{V_0\sigma(\xi)}{4\rho\lambda^2 L \sin\frac{1}{2}\theta\,(1-\xi)\xi + \sigma^2(\xi)}\,.$$

Separating variables, and setting $t = 0$ when $\xi = 0$, the parameter value $\xi_k$ of the reference point at time $t_k = k\Delta t$ is determined by the relation

$$\int_0^{\xi_k} 4\rho\lambda^2 L \sin\tfrac{1}{2}\theta\,\frac{(1-\xi)\xi}{\sigma(\xi)} + \sigma(\xi)\;\mathrm{d}\xi \;=\; V_0\int_0^{k\Delta t}\mathrm{d}t \;=\; V_0 k\Delta t\,. \tag{32}$$

Now since $\sigma(\xi)$ is the derivative of the arc length $s(\xi)$, the indefinite integral of the second term in the integrand on the left is simply $s(\xi)$. To obtain the indefinite integral of the first term, we observe that the parametric speed (16) has the factorization

$$\sigma(\xi) \;=\; \lambda^2 L\,\sigma_+(\xi)\sigma_-(\xi) \tag{33}$$

with

$$\sigma_\pm(\xi) \;=\; (1-\xi)^2 \pm \alpha\,2(1-\xi)\xi + \xi^2\,, \tag{34}$$

where we define

$$\alpha \,=\, \sqrt{\tfrac{1}{2}(1-\cos\tfrac{1}{2}\theta)} \,=\, \sin\tfrac{1}{4}\theta\,, \quad \beta \,=\, \sqrt{\tfrac{1}{2}(1+\cos\tfrac{1}{2}\theta)} \,=\, \cos\tfrac{1}{4}\theta\,. \qquad (35)$$

Consequently, we have the partial fraction decomposition

$$\frac{(1-\xi)\xi}{\sigma(\xi)} \,=\, \frac{1}{4\lambda^2\alpha\, L}\left[\frac{1}{\sigma_-(\xi)} - \frac{1}{\sigma_+(\xi)}\right].$$

Then, since $\sigma_-(\xi)$ and $\sigma_+(\xi)$ both have negative discriminants, we obtain

$$\int \frac{(1-\xi)\xi}{\sigma(\xi)}\,\mathrm{d}\xi \,=\, \frac{1}{4\lambda^2\alpha\beta\, L}\left[\tan^{-1}\frac{(1+\alpha)(2\xi-1)}{\beta} \,-\, \tan^{-1}\frac{(1-\alpha)(2\xi-1)}{\beta}\right].$$

A further simplification becomes possible on invoking [1] the rule

$$\tan^{-1}x - \tan^{-1}y \,=\, \tan^{-1}\frac{x-y}{1+xy} \qquad \text{when } \; xy > -1\,, \qquad (36)$$

and using $\alpha^2+\beta^2=1$, to obtain

$$\int \frac{(1-\xi)\xi}{\sigma(\xi)}\,\mathrm{d}\xi \,=\, \frac{1}{4\lambda^2\alpha\beta\, L}\tan^{-1}\left(\frac{\alpha}{\beta}\,\frac{2\xi-1}{2\xi^2-2\xi+1}\right).$$

Hence, evaluating the definite integral (32) and noting that $2\alpha\beta = \sin\frac{1}{2}\theta$, the reference–point parameter value $\xi_k$ at time $t = k\Delta t$ is the (unique) real root of the function

$$F(\xi) \,=\, 2\rho\left[\tan^{-1}\left(\frac{\alpha}{\beta}\,\frac{2\xi-1}{2\xi^2-2\xi+1}\right) - \tan^{-1}\left(-\frac{\alpha}{\beta}\right)\right] \,+\, s(\xi) \,-\, V_0 k\Delta t\,.$$

Using (36) and $\alpha^2+\beta^2=1$ again, this can be reduced to

$$F(\xi) \,=\, 2\rho\tan^{-1}\left(\frac{2\alpha\beta\,\xi^2}{2\beta^2\xi^2-2\xi+1}\right) \,+\, s(\xi) \,-\, V_0 k\Delta t\,.$$

This function is monotone–increasing with $\xi$, from $F(0) = -V_o k\Delta t$ to $F(1) = \rho\,\theta + S - V_0 k\Delta t$. Its unique real root can be computed to machine precision with a few of the Newton–Raphson iterations (27). The derivative of $F(\xi)$, required in (27), is simply

$$F'(\xi) \,=\, 4\rho\lambda^2\sin\tfrac{1}{2}\theta L\,\frac{(1-\xi)\xi}{\sigma(\xi)} \,+\, \sigma(\xi)\,.$$

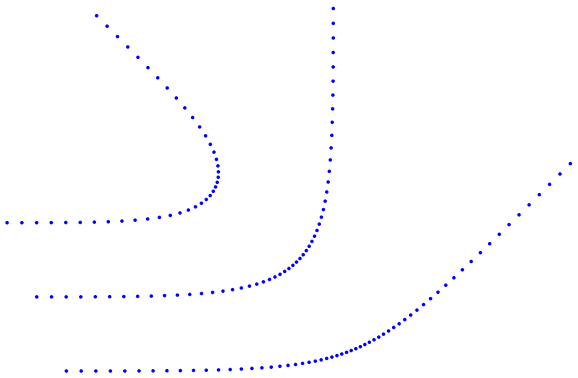

Figure 9: The distribution of reference points along $G^2$ PH quintic corner curves with angles $\theta = \frac{1}{4}\pi,\ \frac{1}{2}\pi,\ \frac{3}{4}\pi$, using the curvature–dependent feedrate (30) with the values $L = 1$ mm, $V_0 = 50$ mm/sec, $\Delta t = 0.001$ sec, and $f = \frac{1}{3}$.

Figure 9 shows typical examples of the distribution of reference points along some $G^2$ PH quintic corner curves, generated in accordance with the feedrate function (30) by the above real–time interpolator procedure.

The traversal time $T$ for the rounded corner, relative to $T_0$, is determined by replacing $\xi_k$ with 1 and $k\Delta t$ with $T$ in (32). This gives

$$\frac{T}{T_0} \;=\; \frac{\rho\,\theta + S}{4L}\,. \tag{37}$$

Note that, if $\rho$ is specified by (31), it has the same sign as the curvature (19) — namely, the sign of the turning angle $\theta$ — and hence $\rho\,\theta > 0$ in (37). The ratio (37) is plotted in Figure 10 for the corner angles $\theta = \frac{1}{4}\pi, \frac{1}{2}\pi, \frac{3}{4}\pi$.

Note that $T/T_0 \to S/4L$ ($< \frac{1}{2}$, since $S \leq 2L$ from (18)) as $\rho \to 0$ — i.e., $f \to 1$. This identifies the case where the nominal feedrate $V_0$ is maintained along the rounded corner. It is evident in Figure 10 that $T/T_0$ increases as $f$ decreases, and at some point exceeds unity — i.e., there is no reduction in cornering time because the curvature–dependent feedrate suppression is too aggressive. From (18), the condition $T < T_0$ can be expressed as

$$\rho\,\theta \;<\; 2L\left[\,1 + \frac{\sin^2\frac{1}{2}\theta}{6\cos\frac{1}{2}\theta + 1}\,\right]\,.$$

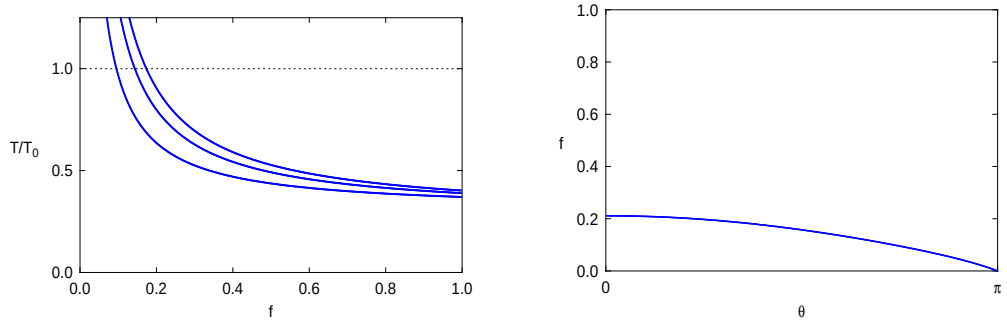


Figure 10: Left: the ratio (37) of corner traversal times plotted as a function of the feedrate reduction ratio $f = V_{\min}/V_0$ for the three corner angles $\theta = \frac{1}{4}\pi$ (upper), $\frac{1}{2}\pi$ (middle), $\frac{3}{4}\pi$ (lower). Right: the minimum $f$ value that ensures reduction in the cornering time ratio (37), as a function of corner angle $\theta$.

Alternatively, using (20) and (31), the fraction $f = V_{\min}/V_0$ must satisfy

$$f \;>\; \frac{15(\cos\frac{1}{2}\theta + 1)^2\theta}{15(\cos\frac{1}{2}\theta + 1)^2\theta + 64(\sin^2\frac{1}{2}\theta + 6\cos\frac{1}{2}\theta + 1)\tan\frac{1}{2}\theta}\,. \tag{38}$$

The variation of this lower bound on $f$ with $\theta$ is illustrated in Figure 10.

For the feedrate (30), the acceleration along the $G^2$ PH quintic corner curve can be determined from (5) — where, from (19) and (30), we have

$$V'(\xi) = -\frac{V_0\rho\,\kappa'(\xi)}{(\rho\,\kappa(\xi)+1)^2}\,, \quad \kappa'(\xi) = 4\lambda^2 L \sin\tfrac{1}{2}\theta\left[\frac{1-2\xi}{\sigma^2(\xi)} - \frac{2(1-\xi)\xi\,\sigma'(\xi)}{\sigma^3(\xi)}\right].$$

Since $\kappa(0) = \kappa(1) = 0$, the normal acceleration is continuous at the junctures of the corner curve with the linear segments. However, since $\kappa'(0)$ and $\kappa'(1)$ are non–zero, the tangential acceleration $A = \mathrm{d}V/\mathrm{d}t$ is discontinuous. From the previous results, the magnitude $\Delta A$ of the feed acceleration discontinuity at the end points, can be expressed as

$$\frac{\Delta A}{A_0} \;=\; \frac{1-f}{f}\;\frac{(6\cos\frac{1}{2}\theta + 1)(\cos\frac{1}{2}\theta + 1)^2}{240\,\cos\frac{1}{2}\theta}\,, \tag{39}$$

where $A_0 = V_0^2/2L$ is the rate of uniform acceleration/deceleration between speeds $V_0$ and 0 over a linear distance $L$. The expression (39) is plotted as a function of $f$ in Figure 11, for corner angles $\theta = \frac{1}{4}\pi, \frac{1}{2}\pi, \frac{3}{4}\pi$. The acceleration

discontinuity is singular as $f \to 0$, but this limit should be avoided to ensure a reduction in cornering time (see Figure 10). In practice, equation (39) can be used to find the minimum $f$ that keeps $\Delta A/A_0$ below a desired threshold.

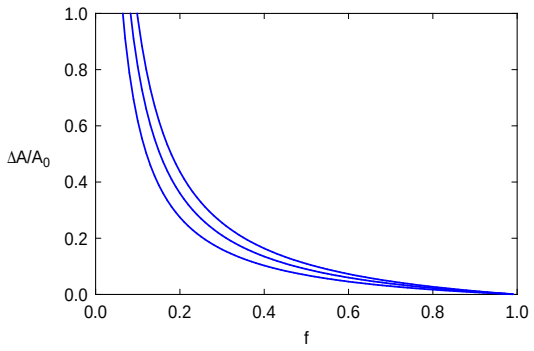


Figure 11: The measure (39) of tangential acceleration discontinuity for the feedrate (30) with corner angles $\theta = \frac{1}{4}\pi$ (upper), $\frac{1}{2}\pi$ (middle), and $\frac{3}{4}\pi$ (lower).

Continuity of tangential acceleration can be achieved by (i) using a higher–order $G^3$ corner curve, with $\kappa'(0) = \kappa'(1) = 0$, together with the feedrate (30); or (ii) using the quintic $G^2$ corner curve, and modifying the feedrate function so that $V'(0) = V'(1) = 0$, as described in the following section.

# 6 Hybrid feedrate function

The feedrate (21) is acceleration continuous, but has no intuitive geometrical interpretation. Although the feedrate (30) is specified in a purely geometrical manner, it does not achieve precise tangential acceleration continuity at the corner end points. We now consider a "hybrid" of the parameter–dependent and curvature–dependent feedrates, specified by multiplying the curvature $\kappa(\xi)$ in (30) with the parameter–dependent modulating factor $4(1-\xi)\xi$, which serves to suppress the tangential acceleration discontinuities — namely

$$V(\xi) \;=\; \frac{V_0}{4\rho\,(1-\xi)\xi\,\kappa(\xi) + 1}\,, \tag{40}$$

where we again have $V_{\min} = V(\frac{1}{2}) = f\,V_0$ when $\rho$ is defined by (31).

Since $\kappa(0) = \kappa(1) = 0$, the normal acceleration term $\kappa(\xi)V^2(\xi)$ in (5) vanishes at the corner curve end points. Moreover, from the derivative

$$V'(\xi) \;=\; -\,\frac{4\,\rho\,V_0\,[\,(1-2\xi)\,\kappa(\xi) + (1-\xi)\xi\,\kappa'(\xi)\,]}{[\,4\,\rho\,(1-\xi)\xi\,\kappa(\xi) + 1\,]^2}$$

of (40), it is evident that $V'(0) = V'(1) = 0$, so the tangential acceleration term $V(\xi)V'(\xi)/\sigma(\xi)$ also vanishes at the corner curve end points. Figure 12 shows the variation of the feedrate (40) with fractional arc length along the $G^2$ PH quintic corner, for several $f$ values (the corner angle $\theta = \frac{1}{2}\pi$ is shown here: the cases $\theta = \frac{1}{4}\pi$ and $\frac{3}{4}\pi$ are qualitatively similar).

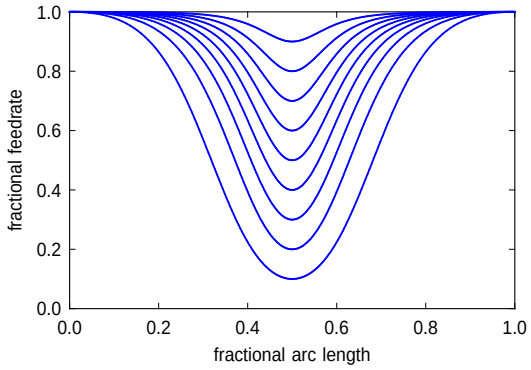


Figure 12: Fractional feedrate $V/V_0$ versus arc length $s/S$ for the hybrid feedrate function (40) with the values $f = V_{\min}/V_0 = 0.1, \ldots, 0.9$.

For the hybrid feedrate (40), the differential equation (24) becomes

$$\frac{\mathrm{d}\xi}{\mathrm{d}t} \;=\; \frac{V_0\,\sigma(\xi)}{16\rho\lambda^2 L \sin\frac{1}{2}\theta\,(1-\xi)^2\xi^2 + \sigma^2(\xi)}\,,$$

and on separating variables and integrating, this yields

$$\int_0^{\xi_k} 16\rho\lambda^2 L \sin\tfrac{1}{2}\theta\,\frac{(1-\xi)^2\xi^2}{\sigma(\xi)} + \sigma(\xi)\;\mathrm{d}\xi \;=\; V_0 k\Delta t\,. \tag{41}$$

The indefinite integral of $\sigma(\xi)$ is again just $s(\xi)$, and the factorization of $\sigma(\xi)$ specified by (33)–(35) yields the partial fraction decomposition

$$\frac{(1-\xi)^2\xi^2}{\sigma(\xi)} \;=\; \frac{1}{8\lambda^2\alpha\beta^2 L}\left[\frac{1-\alpha}{\sigma_-(\xi)} - \frac{1+\alpha}{\sigma_+(\xi)} + 2\alpha\right].$$

For brevity, we now set

$$\zeta \;=\; \frac{1+\alpha}{\beta} \quad \text{and} \quad \eta \;=\; \frac{1-\alpha}{\beta}\,, \tag{42}$$

and note that $\zeta\eta = 1$, since $\alpha^2 + \beta^2 = 1$. The preceding expression then has the indefinite integral

$$\int \frac{(1-\xi)^2\xi^2}{\sigma(\xi)}\,\mathrm{d}\xi \;=\; \frac{\eta\tan^{-1}\zeta(2\xi-1) - \zeta\tan^{-1}\eta(2\xi-1) + 2\,\alpha\,\xi}{8\lambda^2\alpha\beta^2 L}\,.$$

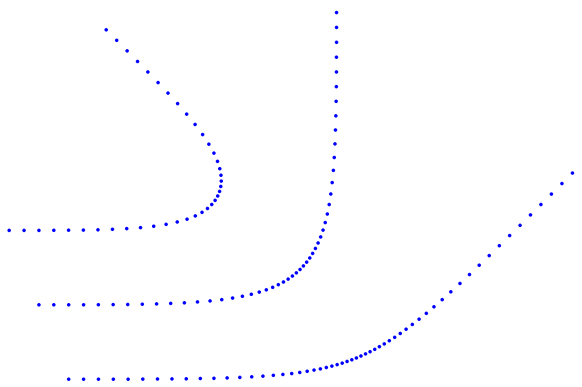

Figure 13: The distribution of reference points along $G^2$ PH quintic corner curves with angles $\theta = \frac{1}{4}\pi,\ \frac{1}{2}\pi,\ \frac{3}{4}\pi$, using the hybrid feedrate (40) with the values $L = 1$ mm, $V_0 = 50$ mm/sec, $\Delta t = 0.001$ sec, and $f = \frac{1}{3}$.

Hence, evaluating the definite integral (41) and noting that $2\alpha\beta = \sin\frac{1}{2}\theta$, the parameter value $\xi_k$ at time $t = k\Delta t$ is the real root of the function

$$F(\xi) = \frac{4\rho}{\beta}\left[\,\eta\tan^{-1}\zeta(2\xi-1) - \zeta\tan^{-1}\eta(2\xi-1) + 2\alpha\xi + \gamma\,\right] + s(\xi) - V_0 k\Delta t$$

where

$$\gamma \;=\; \eta\tan^{-1}\zeta - \zeta\tan^{-1}\eta\,.$$

The function $F(\xi)$ is monotone–increasing with $\xi$, from $F(0) = -V_0 k\Delta t$ to $F(1) = 8\rho(\alpha+\gamma)/\beta + S - V_0 k\Delta t$. Its unique real root can be computed to machine precision by just a few of the Newton–Raphson iterations (27), with the starting value (28). The derivative of $F(\xi)$, required in (27), is simply

$$F'(\xi) \;=\; 16\rho\lambda^2\sin\tfrac{1}{2}\theta L\,\frac{(1-\xi)^2\xi^2}{\sigma(\xi)} \;+\; \sigma(\xi)\,.$$

Figure 13 shows typical examples of the distribution of reference points along some $G^2$ PH quintic corner curves, generated in accordance with the feedrate function (40) by the above real–time interpolator algorithm.

For the hybrid feedrate function (40), the corner traversal time ratio is

$$\frac{T}{T_0} \;=\; \frac{8\rho(\alpha+\gamma)+\beta S}{4\beta L}\,. \tag{43}$$

It can be verified that $\alpha+\gamma$ has the same sign as $\rho$, so the product $\rho(\alpha+\gamma)$ is always positive. The ratio (43) is plotted in Figure 14 for corner angles $\theta = \frac{1}{4}\pi, \frac{1}{2}\pi, \frac{3}{4}\pi$ — the behavior is qualitatively similar to that in Figure 10 for the feedrate function (30), although (40) admits somewhat smaller $f$ values for a given reduction in cornering time. As with (30), we have $T/T_0 \to S/4L < \frac{1}{2}$ as $f \to 1$ for (40). Because of the complicated dependence of the left–hand side of (43) on $\theta$, it is more difficult in this case to formulate a bound on $f$, analogous to (38), that ensures a reduction in cornering time.

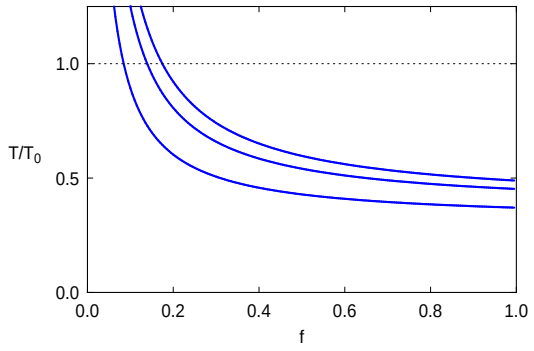


Figure 14: The ratio (43) of corner traversal times as a function of the ratio $f = V_{\min}/V_0$ for the corner angles $\theta = \frac{1}{4}\pi$ (upper), $\frac{1}{2}\pi$ (middle), $\frac{3}{4}\pi$ (lower).

# 7 Acceleration analysis

From (4) and (5), the acceleration can be expressed in complex form as

$$\mathbf{a}(\xi) \;=\; \frac{\mathbf{f}(\xi)}{\sigma^3(\xi)}\,, \quad \mathbf{f}(\xi) \;=\; V(\xi)\,[\,\sigma(\xi)V'(\xi) + 2\,\mathrm{i}\,h(\xi)V(\xi)\,]\,\mathbf{w}^2(\xi)\exp(\mathrm{i}\phi)\,,$$

where $h(\xi)$ is the quadratic polynomial

$$h(\xi) \;=\; \mathrm{Im}(\overline{\mathbf{w}}(\xi)\mathbf{w}'(\xi)) \;=\; u(\xi)v'(\xi) - u'(\xi)v(\xi)\,,$$

and, as indicated in Section 3, the factor $\exp(\mathrm{i}\phi)$ accounts for a general corner curve orientation. The real and imaginary parts of $\mathbf{a}(\xi)$ specify the $x$ and $y$ axis accelerations $a_x(\xi)$ and $a_y(\xi)$. For brevity, we shall consider here only the parameter–dependent feedrate function (21) — similar principles apply to the feedrate functions (30) and (40), but the analysis is more involved.

In the case of the feedrate (21), $\mathbf{w}(\xi)$ is quadratic, $\sigma(\xi)$ is quartic, $h(\xi)$ is quadratic, and $V(\xi)$ is quintic, so the complex polynomial $\mathbf{f}(\xi)$ is degree 17. Differentiating $\mathbf{a}(\xi)$ gives

$$\mathbf{a}'(\xi) \;=\; \frac{\mathbf{g}(\xi)}{\sigma^4(\xi)}\,, \quad \mathbf{g}(\xi) \;:=\; \sigma(\xi)\mathbf{f}'(\xi) - 3\sigma'(\xi)\mathbf{f}(\xi)\,,$$

where $\mathbf{g}(\xi)$ is a complex polynomial of degree 20, that can be constructed in a numerically–stable manner using the addition and multiplication rules for polynomials in Bernstein form [8, 17]. The $x$ and $y$ axis acceleration extrema occur at the real roots on $\xi \in [\,0, 1\,]$ of the real polynomials

$$g_x(\xi) \;=\; \mathrm{Re}(\mathbf{g}(\xi)) \quad \text{and} \quad g_y(\xi) \;=\; \mathrm{Im}(\mathbf{g}(\xi))\,.$$

These roots can be computed to machine precision using the subdivision and variation–diminishing properties of the Bernstein form.

# 8 Closure

A family of planar PH quintic curves, suitable for rounding the sharp corners of piecewise–linear toolpaths to a specified tolerance and with $G^2$ continuity, has been introduced. The PH corner curves are accompanied by a repertoire of continuously–variable feedrates that can be exploited to suppress cornering accelerations within safe bounds. Each feedrate function is characterized by two intuitive parameters: the entry/exit feedrate $V_0$, and feedrate suppression factor $f = V_{\min}/V_0$ expressing the minimum (i.e., mid–point) feedrate $V_{\min}$ as a fraction of $V_0$. Moreover, each feedrate function admits a closed–form reduction of the interpolation integral, facilitating the development of highly accurate and efficient real–time interpolator algorithms.

The companion paper [11] presents a detailed experimental performance analysis for this corner–rounding strategy, including the acceleration–limited selection of feedrate parameters for the rounded corner curves and the linear segments between them, through implementation on a 3–axis CNC machine with an open–architecture controller. This implementation demonstrates the significant practical benefits of the proposed cornering scheme over the simple "full stop" method for exact execution of sharp corners.

# References


[1] I. N. Bronshtein, K. A. Semendyayev, G. Musiol, and H. Muehlig (2004), *Handbook of Mathematics* (4th edition), Springer, Berlin.

[2] C. A. Ernesto and R. T. Farouki (2012), High–speed cornering by CNC machines under prescribed bounds on axis accelerations and toolpath contour error, *Int. J. Adv. Manuf. Tech.* **58**, 327–338.

[3] R. T. Farouki (1994), The conformal map $z \rightarrow z^2$ of the hodograph plane, *Comput. Aided Geom. Design* **11**, 363–390.

[4] R. T. Farouki (2008), *Pythagorean–Hodograph Curves: Algebra and Geometry Inseparable*, Springer, Berlin.

[5] R. T. Farouki, J. Manjunathaiah, and S. Jee (1998), Design of rational cam profiles with Pythagorean–hodograph curves, *Mech. Mach. Theory* **33**, 669–682.

[6] R. T. Farouki, J. Manjunathaiah, D. Nicholas, G.–F. Yuan, and S. Jee (1998), Variable feedrate CNC interpolators for constant material removal rates along Pythagorean–hodograph curves, *Comput. Aided Design* **30**, 631–640.

[7] R. T. Farouki, J. Manjunathaiah, and G.–F. Yuan (1999), G codes for the specification of Pythagorean–hodograph tool paths and associated feedrate functions on open–architecture CNC machines, *Int. J. Mach. Tools Manuf.* **39**, 123–142.

[8] R. T. Farouki and V. T. Rajan (1988), Algorithms for polynomials in Bernstein form, *Comput. Aided Geom. Design* **5**, 1–26.

[9] R. T. Farouki and T. Sakkalis (1990), Pythagorean hodographs, *IBM J. Res. Develop.* **34**, 736–752.

[10] R. T. Farouki and S. Shah (1996), Real–time CNC interpolators for Pythagorean–hodograph curves, *Comput. Aided Geom. Design* **13**, 583–600.

[11] K. M. Nittler and R. T. Farouki (2015), Efficient high–speed cornering motions based on continuously–variable feedrates. II. Implementation and performance analysis, preprint.

[12] B. Sencer, K. Ishikazi, and E. Shamoto (2015), A curvature optimal sharp corner smoothing algorithm for high–speed feed motion generation of NC systems along linear tool paths, *Int. J. Adv. Manuf. Tech.* **76**, 1977–1992.

[13] J. Shi, Q. Z. Bi, Y. H. Wang, and G. Liu (2014), Development of real–time look–ahead methodology based on quintic PH curve with $G^2$ continuity for high–speed machining, *Appl. Mech. Mater.* **464**, 258–264.

[14] J. Shi, Q. Bi, L. Zhu, and Y. Wang (2015), Corner rounding of linear fixed–axis tool path by dual PH curves blending, *Int. J. Mach. Tools Manuf.* **88**, 223–236.

[15] Z. Šír and B. Jüttler (2005), Constructing acceleration continuous tool paths using Pythagorean hodograph curves, *Mech. Mach. Theory* **40**, 1258–1272.

[16] Z. Šír, E. Wings, and B. Jüttler (2007), Rounding spatial G code tool paths using Pythagorean hodograph curves, *Trans. ASME J. Comput. Inf. Sci, Eng.* **7**, 186–191.

[17] Y–F. Tsai and R. T. Farouki (2001), Algorithm 812: BPOLY: An object–oriented library of numerical algorithms for polynomials in Bernstein form, *ACM Trans. Math. Software* **27**, 267–296.

[18] Y–F. Tsai, R. T. Farouki, and B. Feldman (2001), Performance analysis of CNC interpolators for time–dependent feedrates along PH curves, *Comput. Aided Geom. Design* **18**, 245–265.

[19] D. J. Walton and D. S. Meek (2009), $G^2$ blends of linear segments with cubics and Pythagorean–hodograph quintics, *Int. J. Comput. Math.* **86**, 1498–1511.